Microstructures and Mechanical Properties of Spark Plasma Sintered Al$_2$O$_3$-Co Composites Using Electroless Deposited Al$_2$O$_3$-Co Powders

Byong-Taek Lee*, Ki-Ho Kim, A. H. M. Esfakur Rahman and Ho-Yeon Song

Department of Biomedical Engineering and Materials, School of Medicine, Soonchunhyang University,
366-1 Ssangyoung-dong, Cheonan City, Chungnam 330-090, Korea

Microstructures and mechanical properties of spark plasma sintered (SPS) Al$_2$O$_3$-Co composites were investigated depending on the sintering temperatures (900–1200°C) and cobalt contents (0∼12 mass%). The material properties of relative density and fracture toughness increased as the sintering temperature and Co content (up to 12 mass%Co) increased. In the SPSed Al$_2$O$_3$-Co composite sintered at 1200°C, maximum values of relative density and fracture toughness about 99.3% and 8.1 MPam$^{1/2}$, respectively were obtained. The fracture morphology of SPSed Al$_2$O$_3$-12 mass%Co composite showed a semi-brittle fracture mode due to the homogeneous dispersion of fine-sized Co particles. [doi:10.2320/matertrans.MRA2008015]

1. Introduction

Aluminum ceramic (Al$_2$O$_3$) has been widely used as a typical engineering material due to its excellent wear resistance, high elastic modulus, and good chemical properties as well as its reasonable cost in the fabrication process.[1,2] Recently, Al$_2$O$_3$ has also been used as a biomaterial such as dental materials, total hip prostheses and replacement of various parts of the human body due to its good biocompatibility as well as its excellent material properties. To improve the fracture toughness of Al$_2$O$_3$ ceramic, many researchers have focused on the fabrication of composites by the addition of hard ceramic phases such as TiC and ZrO$_2$ particles, SiC whisker and fiber reinforcements.[3,4] In these composites, micro-cracking,[5] crack bridging[6] and crack deflection[7] and stress induced phase transformation mechanisms were found.[5] However, the wide application of Al$_2$O$_3$ ceramic has been limited because its fracture toughness was not improved remarkably.[8] Thus, as a different approach, there have been many reports on the ceramic/metal composites in which metal particles were dispersed in the Al$_2$O$_3$ matrix to introduce the plastic deformation mechanism by the dispersion of ductile phases such as Ni, Ni-P, Mo and Ag particles.[9–12]

They can remarkably reduce the stress concentration in the notches/microcracks due to the plastic deformation. The Co alloy has been already used for dental implants due to its good biocompatibility.[13] Furthermore, the attractive point for making the Al$_2$O$_3$ composite is its high melting point (1495°C) compared with that of other metallic systems.

There have been many reports on the fabrication of ceramic/metal composites such as attrition milling,[14] sol-gel,[15] ball milling[16] and electroless deposition processes.[9] Among them, the electroless deposition process is understood as an excellent method to synthesize the homogeneous ceramic/metal composites.[17,18] This method allows easy control of coating thickness, even dispersion of nano sized metal coating and a homogeneous distribution of all components without dependency on the chemical compositions. It is especially important in the ceramic/metal composites that the metal phase should be controlled with fine sized particles to reduce the formation of cracking, which is due to the mismatch of thermal expansion coefficients between the ceramic and metal phases.

Recently, nano ceramics having nano-crystalline grains has been actively investigated.[19] For the fabrication of nano crystalline sintered bodies, the spark plasma sintering (SPS) technique has been widely used because it has some advantages such as the easy, fast heating process and low temperature sintering compared with that of conventional sintering techniques.

In this study, Co coated Al$_2$O$_3$ powders synthesized by the electroless deposition process were used as a starting material. This work focused on the relationship between the microstructure and material properties of SPSed Al$_2$O$_3$-Co composites depending on the Co contents and sintering temperature.

2. Experimental Procedure

Co coated Al$_2$O$_3$ powders were synthesized by the electroless deposition process. For the coating of nano-crystalline Co, the cobalt sulfate heptahydrate (CoSO$_4$· 7H$_2$O, Samchun Pure Chemical Company Ltd. Korea) as the cobalt source, sodium phosphinate monohydrate (NaH$_2$PO$_2$·H$_2$O, Junsei Chemical Co. Ltd. Japan) as the reducing agent, sodium citrate dehydrate (C$_6$H$_5$O$_7$Na$_3$· 2H$_2$O, Samchun Pure Chemical Co. Ltd, Korea) as the complexing agent and boric acid (H$_3$BO$_3$, Samchun Pure Chemical Co. Ltd. Korea) as the stabilizer, were used. The composition of Co coating solutions used was the following; 21 g/L of NaH$_2$PO$_2$·H$_2$O, 115 g/L of C$_6$H$_5$O$_7$Na$_3$· 2H$_2$O, 30 g/L of H$_3$BO$_3$ and then the concentration of CoSO$_4$·7H$_2$O was varied as 15 g/L, 30 g/L and 45 g/L. α-Al$_2$O$_3$ powders (30 g, AKP-50, Sumitomo Chem. Co., Japan) with about 300 nm in diameter were added to the Co plating solution. The temperature of the coating bath was maintained at 90°C and the pH of the bath was maintained at

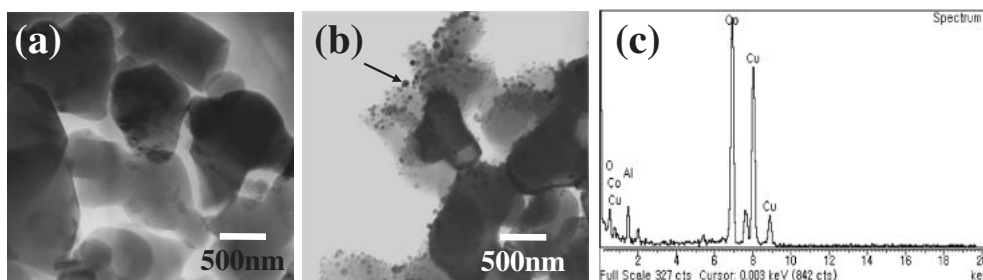*Corresponding author, E-mail: lbt@sch.ac.kr

Fig. 1   TEM micrographs of (a) raw Al_2O_3, (b) calcined Al_2O_3 powders after Co electroless deposition and (c) EDS profile.

11 by the addition of sodium hydroxide (NaOH). According to the concentration of $CoSO_4 \cdot 7H_2O$, the synthesized Co deposits measured by ICP-AES (ICP-IRIS, Thermal Jarrell Ash, USA) were 3.9 mass%, 8.4 mass% and 12.4 mass%, respectively which will be rounded to 4, 8, 12 mass% in this paper. To eliminate the residual organic component of the coating process, the Co coated Al_2O_3 powders were washed several times using a diluted hydrochloric acid solution and de-ionized water. To neutralize the Co coated Al_2O_3 powders, the washing was carried out repeatedly with diluted sulfuric acid (H_2SO_4) and rinsed with de-ionized water using a suction system and then dried at 80°C for 6 hours. The dried powders were calcined at 900°C in Argon (Ar) atmosphere for 1 h. For densification of the Co coated Al_2O_3 powder, the sintering was carried out at 900, 1000, 1100 and 1200°C for 2 minutes in Ar atmosphere under applied pressure of 30 MPa at 50°C/min. The phase analysis of Al_2O_3 powder, calcined Al_2O_3-Co powder and Al_2O_3-Co sintered composites was identified using an X-ray diffractometer (XRD, D/MAX-250, Rigaku, Japan) with CuKα radiation ($\lambda = 0.154056$ nm). FE-SEM (Sirion, FEI, Netherlands) and TEM (JEM 2010, JEOL, Japan) techniques were used to observe the detailed microstructures and fracture surfaces. The relative density was measured by the Archimedes method, and the Vickers hardness and fracture toughness were measured by the indentation method using loads of 4.9 N and 98 N, respectively.

3.   Results and Discussion

Figure 1 shows TEM images of (a) the raw Al_2O_3 powder and (b) the calcined Al_2O_3 powder after Co coating by the electroless deposition process, respectively. The raw Al_2O_3 powder shows a round shape about 300–500 nm in diameter as shown in Fig. 1(a). In Figure 1(b), it could be clearly observed that the Al_2O_3 powder was successfully coated with Co nanoparticles of 5–15 nm in diameter. Most of the Co particles homogeneously adhered to the Al_2O_3 powders. From the EDS spectrum taken from an arrow in Fig. 1(b), Al and Co peaks were found and the intensity of the Co peak was stronger than that of the Al. In the EDS spectrum, the appearances of Cu peaks were due to using a Cu grid for the preparation of the TEM sample.

To identify the crystal phases of raw powders synthesized by the electroless deposition process and SPSed Al_2O_3-Co composites, XRD analysis was carried out. Figure 2 shows the XRD patterns of (a) raw Al_2O_3 powder, (b) as synthesized Al_2O_3-Co powder, (c) calcined Al_2O_3-Co powder synthe-
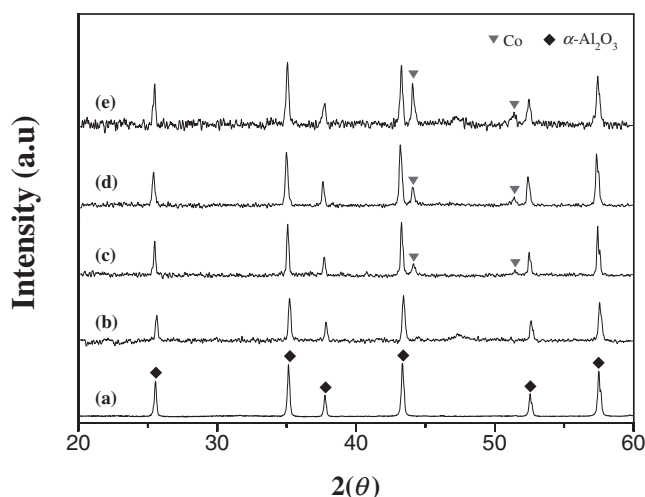
Fig. 2   XRD patterns of (a) raw Al_2O_3, (b) as-received Al_2O_3-Co powders, (c) calcined Al_2O_3-Co powder, (d) Al_2O_3-4 mass%Co and (e) Al_2O_3-12 mass%Co SPSed composites.

sized by electroless deposition and (d, e) SPSed Al_2O_3-Co composites depending on the Co content. In the as received Co coated Al_2O_3 powder, the main peaks were identified with the Al_2O_3 phase having a rhombohedral structure and no Co peaks were detected. However, after calcination at 900°C (c), Co peaks were detected. From these results, we can understand that in the as-received Co coated Al_2O_3 powder; the Co phase existed with an amorphous structure. On the other hand, in the SPSed bodies containing 4 mass% and 12 mass% Co phase (d, e), the intensity of Co peaks increased remarkably as the Co content increased.

Figure 3 shows TEM micrographs of SPSed Al_2O_3-Co composites sintered at 1100°C, which contained (a) 4 mass%Co and (b) 12 mass%Co. In the Al_2O_3-4 mass%Co composite, many pores were observed due to the low relative density as indicated by arrows. The Co particles (comparatively dark contrast) were observed with fine size less than about 100 nm in diameter. On the other hand, in the SPSed Al_2O_3-12 mass%Co composite (b), the dense microstructure was observed and it was compared with that of Al_2O_3-4 mass%Co composites although the size of Al_2O_3 grains (about in range of 200–450 nm in diameter) was not changed. The remarkable observation was that the Co particles grew less than 300 nm in diameter.

Figure 4 shows the relative density and fracture toughness of SPSed Al_2O_3-Co composites depending on the Co content. The value of relative density gradually increased as the Co
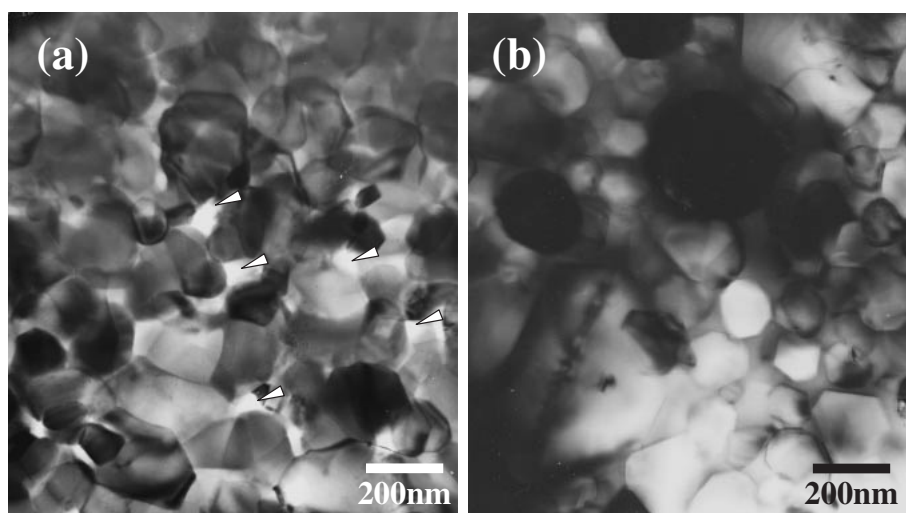
Fig. 3   TEM micrographs of Al$_2$O$_3$-Co SPSed composites at 1100°C depending on the Co content (a) Al$_2$O$_3$-4 mass%Co and (b) Al$_2$O$_3$-12 mass%Co.

content increased, and its maximum value of about 98.9% was obtained in the Al$_2$O$_3$-12 mass%Co composite. The fracture toughness (about 3.12 to 6.35 MPa·m$^{1/2}$) also increased as the Co content increased. That is about twice as high as that of monolithic Al$_2$O$_3$ body (2.6 MPa·m$^{1/2}$). This result indicates that the dispersion of Co particles in the Al$_2$O$_3$ matrix played a significant role in reducing crack propagation energy.

Figure 5 shows the TEM micrographs of SPSed Al$_2$O$_3$-12 mass%Co composites depending on the sintering temperature. In the sample sintered at 900°C (a), many pores (white regions) were observed as indicated by arrows, and most of Al$_2$O$_3$ grains have an ellipsoid shape. These residual pores were appeared during sintering process due to the low temperature sintering as well as the short duration time of SPS process. The comparatively dark contrast regions correspond to the Co grains as indicated with arrows. The Co particles were homogeneously dispersed in Al$_2$O$_3$ matrix, and the average grain sizes of Co and Al$_2$O$_3$ grains were about less than 80 nm and 350 nm in diameter, respectively.

Fig. 4   Material properties of Al$_2$O$_3$-Co SPSed bodies depending on the Co content.

Fig. 5   TEM micrographs of Al$_2$O$_3$-12 mass%Co SPSed composites depending on the sintering temperature (a) 900°C and (b) 1200°C.

However, at 1200°C (b), the microstructure was remarkably changed compared with that of 900°C; i.e., the residual pores were hardly observed due to the full densification. The Al_2O_3 and Co grains were shows about 200–450 and about 150–250 nm in diameter, respectively. Although most Al_2O_3-Co grain interfaces were free of microcracks, large microcracks were observed around agglomerated Co regions, due to the thermal expansion coefficient mismatch between the Al_2O_3 and Co phases. The inserted electron diffraction pattern was taken from the [011] zone axis of a Co grain (marked P) in Fig. 5(b) revealing that the Co phase in the SPSed Al_2O_3-Co composite has a FCC crystal structure.

Figure 6 shows the relative density, Vickers hardness and fracture toughness of SPSed Al_2O_3-12 mass%Co composites dependi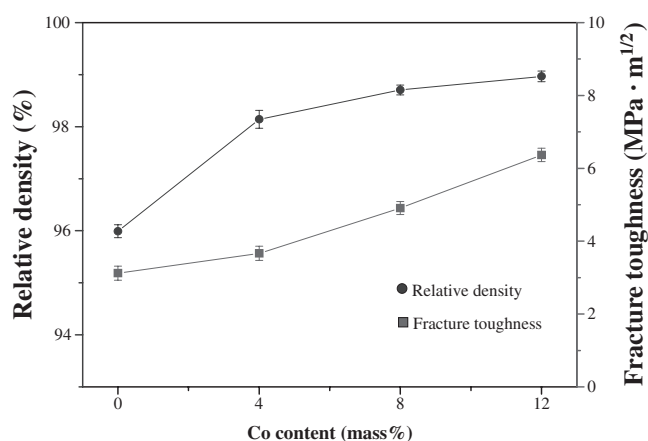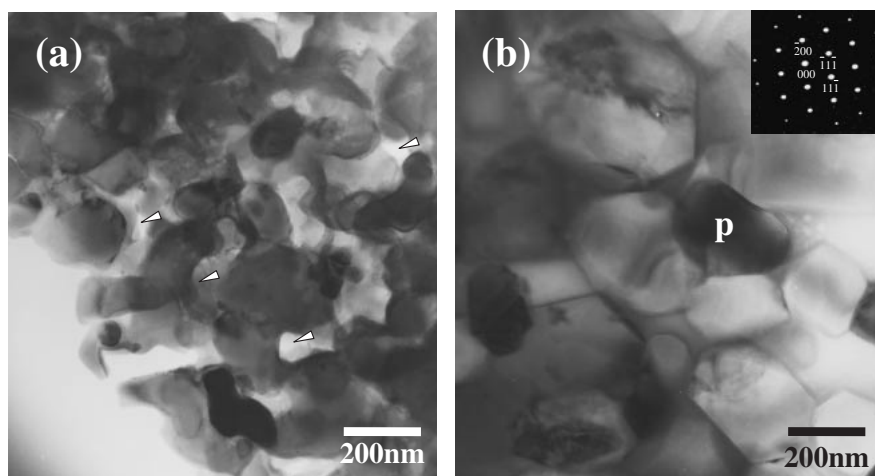ng on the sintering temperature. In the sample sintered at 900°C, the relative density showed low value due to the low temperature sintering as mentioned in Fig. 5. However, this value increased from 92.4% to 99.3% as increasing the sintering temperature of 900°C to 1200°C. The hardness increased with increasing sintering temperature up to 1874 kg/mm² or 18.74 GPa at 1200°C. This value is almost same level with that of Al_2O_3-ZrO_2 composite and the reason for showing with high value is due to the grain refinement of Al_2O_3 and Co phases by the SPS process. Especially, at 1200°C, the fracture toughness was high value with about 8.1 MPam$^{1/2}$ which is over 2 times higher than that of pressureless sintered Al_2O_3 (2.6 MPam$^{1/2}$).[9]

In general, the dispersion of ductile phases in the ceramic matrix could efficiently reduce the crack propagation energy and they led a tendency of transgranular fracture mode.[20] To investigate the fracture characteristic and main reason for the improvement of fracture toughness of SPSed Al_2O_3-12 mass%Co composites, SEM fracture surfaces were observed depending on the sintering temperature. Figure 7 shows the fracture surfaces of Al_2O_3-12 mass%Co SPSed composites. In the SPSed sample at 900°C, many residual pores were observed in the fracture surface as mention in Fig. 5(a) and the main fracture mode was a mixed type with intergranular and transgranular types which were frequently appeared in the typical brittle ceramics. However, as increasing sintering temperature, the fracture mode was remarkably changed with dense surface. Especially, in the samples sintered 1200°C, the main fracture behavior was changed into semi-brittle fracture mode with highly rough surface and transgranular fracture was clearly observed although the intergranular fracture also observed at same local regions. This changing of fracture behavior is basically due to the homogeneous dispersion of Co phase and high densification of Al_2O_3-12 mass%Co composites. Consequently, the dispersion of nano size Co particles in the Al_2O_3 matrix can be acted as an excellent fracture toughening agent by the introducing the crack bridging[6] and plastic deformation[21] of Co particles.

4. Conclusions

Using the nano Co coated Al_2O_3 powders, Al_2O_3-Co composites were fabricated by the SPS process and the relationship between microstructure and fracture behavior was investigated. In the calcined Al_2O_3-Co composite powders, the Co particles in range of 5–15 nm in diameter were homogeneously adhered on the Al_2O_3 raw powders. In the SPSed Al_2O_3-Co composites, the materials properties increased remarkably as increasing the Co content as well as the sintering temperature. Especially, in the SPSed Al_2O_3-12 mass% composite sintered at 1200°C, the maximum values of relative density, hardness and fracture toughness were 99.3%, 1874 Hv and 8.1 MPam$^{1/2}$, respectively. The fracture behavior also remarkably changed from the brittle fracture to semi-brittle mode as increasing the Co content and sintering temperature. The main reason for the significant improvement of fracture toughness was due to the plastic

Fig. 6 Material properties of Al_2O_3-12 mass%Co SPSed composites depending on the sintering temperature.

Fig. 7   SEM fracture surface micrographs of Al_2O_3-Co SPSed bodies depending on the sintering temperatures (a) 900°C and (b) 1200°C.

deformation and crack bridging mechanism by the homogeneous dispersion of fine Co particles as well as the high densification of Al$_2$O$_3$-Co composite.

Acknowledgements

REFERENCES

1) T. C. Wang, R. Z. Chen and W. H. Tuan: J. Eur. Ceram. Soc. **23** (2003) 927–934.
2) P. G. Rao, M. Iwasa, T. Tanaka, I. Kondoh and T. Inoue: Scr. Mater. **48** (2003) 437–441.
3) G. Pezzotti and W. H. Muller: Compu. Mater. Sci. **22** (2001) 155–168.
4) H. J. Chen, W. M. Rainforthe and W. E. Lee: Scr. Mater. **42** (2000) 555–560.
5) B. T. Lee, D. H. Jang, I. C. Kang and C. W. Lee: J. Am. Ceram. Soc. **88** (2005) 2874–2878.
6) L. Jia, G. H. Yu, S. R. Xia and Y. Y. Sheng: Ceram. Inter. **33** (2007) 811–814.
7) B. T. Lee, K. H. Kim and J. K Han: J. Mater. Res. **19** (2004) 3234–3241.
8) S. Scheppokat, R. Hannink, R. Janssen, G. de Portu and N. Claussen: J. Eur. Ceram. Soc. **25** (2005) 837–845.
9) I. H. Oh, J. Y. Lee, J. K. Han, H. J. Lee and B. T. Lee: Surf. Coat. Technol. **192** (2005) 39–42.
10) N. K. Shrestha, D. B. Hamal and T. Saji: Surf. Coat. Technol. **183** (2004) 247–253.
11) O. Sbaizero and G. Pezzotti: Acta Mater. **48** (2000) 985–992.
12) G. M. Shi, J. K. Han, Z. D Zhang, H. Y. Song and B. T. Lee: Surf. Coat. Tehcnol. **195** (2005) 333–337.
13) S. T. Oh, M. Sando and K. Niihara: Scr. Mater. **39** (1998) 1413–1418.
14) C. Zhang, R. Janssen and N. Claussen: Mater. Lett. **57** (2003) 3352–3356.
15) Y. L. Huang, D. S. Xue, P. H. Zhou, Y. Ma and F. S. Li: Mater. Sci. Eng. A **359** (2003) 332–337.
16) J. Li, F. Li and K. Hu: J. Mater. Process Tech. **147** (2004) 236–240.
17) R. Ramaseshan, S. K. Seshadri and N. G. Nair: Scr. Mater. **45** (2001) 183–189.
18) T. N. Khoperia, T. J. Tabatadze and T. I. Zedginidze: Electrochimica Acta. **42** (1997) 3049–3055.
19) Y. Sakabe, Y. Yamashita and H. Yamamoto: J. Eur. Ceram. Soc. **25** (2005) 2739–2742.
20) J. Lu, L. Gao, J. Sun, L. Gui and J. Guo: Mater. Sci. Eng. A **239** (2000) 223–228.
21) J. Li, J. Sun and L. Huang: Mater. Sci. Eng. A **323** (2002) 17–20.